Available online at www.sciencedirect.com
SCIENCE DIRECT®
Journal of Power Sources 132 (2004) 1–10
JOURNAL OF POWER SOURCES
www.elsevier.com/locate/jpowsour

Comparison of dissolution behavior and ionic conduction between Sr and/or Mg doped $LaGaO_3$ and $LaAlO_3$

Te-Yuan Chen, Kuan-Zong Fung*

Department of Materials Science and Engineering, National Cheng Kung University, #1 University Road, Tainan 70101, Taiwan

Received 8 September 2003; accepted 24 December 2003

Abstract

The dissolution of divalent cations plays an important role in the enhancement of conductivity for perovskite-based $LaAlO_3$ and $LaGaO_3$ oxygen conductors. In the $LaAlO_3$ system, the solubility of MgO was less than 10% due to the mismatch of ionic radius between the Mg and Al cations. The substitution of Sr ions in the La-cation sublattice was as high as 20%. With the doubly-doping of SrO and MgO in $LaAlO_3$, the enhancement of MgO solubility was also observed. However, further addition of MgO tends to lower the solubility of Sr ion from 20 to 10%. This result can be rationalized by the reduced distance between Mg ion and Sr ion that caused the cation–cation repulsion in the perovskite structure. In the singly-doped $LaGaO_3$ systems, the solubility of MgO was found to be 20%. However, only less than 10% of the La-cation sublattice could be substituted by Sr ions. With the doubly-doping of SrO and MgO, the solubility of SrO was significantly enhanced by the addition of MgO. It is believed that the solubility enhancement of SrO is due to the expanded lattice caused by the addition of MgO. Within the solubility limit of the aliovalent cations, the ionic conductivities of both $LaAlO_3$ and $LaGaO_3$ systems increased with the increasing concentration of foreign cations. After the solubility limits in both doped $LaAlO_3$ and $LaGaO_3$ were reached, the segregation of the second phase tends to lower the ionic conductivity drastically. The activation energy for ionic conduction was also dependent on the ionic radius of foreign cations which may affect the space available for the transport of oxygen ions.

Keywords: $LaAlO_3$; $LaGaO_3$; Solid electrolyte; Conductivity; SOFCs

1. Introduction

Oxygen ion conductors are the key electrolyte components in many solid electrochemical devices such as oxygen sensors, oxygen pumps and solid oxide fuel cells (SOFCs). SOFC offers a clean, pollution-free alternative energy source for the electrochemical generation of electricity at high efficiency. Solid electrolytes for SOFCs have been focused on fluorite-structured ZrO_2, CeO_2, and Bi_2O_3 [1–4].

Although yttria stabilized zirconia (YSZ) has been widely used as the electrolyte material for SOFC applications, the oxide ion conductivity of YSZ is rather low for intermediate-temperature operation. Thus, SOFCs which use YSZ electrolytes must operate at around 1000 °C. Such a high temperature leads to problems associated with high costs and the connected materials at the operating temperature. In particular, there are problems associated with phase stability of the various component materials and their compatibility at ~1000 °C. Doped Bi_2O_3 and CeO_2, on the other hand, have shown much improved ionic conductivity. Nevertheless, they exhibit some electronic conduction under the reducing atmospheres. For low-temperature SOFC applications, it is necessary for solid electrolyte to possess adequate stability and high ionic conductivity.

To search for a new electrolyte with higher conductivity and better stability, perovskite-type oxides (ABO_3) have received much attention because this unique structure is very tolerant of various sizes of cations at both A and B cation sublattices. Thus, aliovalent cations can be dissolved in both A-site and B-site cation sublattices. Consequently, oxygen vacancies are generated to compensate the charge of substituting ions. In other words, perovskite-type oxides offer numerous advantages, especially for the stability of the crystal structure, the variety of elements that can be accommodated in the crystal lattice, and the ease with which oxygen vacancies can be produced by partial substitution of the A- and/or B-site cations with lower valence cations.

Several oxides with perovskite structures have been studied as potential oxide ion conductors. Among them, $LaGaO_3$-based oxides [5–11] have been investigated for the

* Corresponding author. Tel.: +886-6-2380208; fax: +886-6-2346290/2380208.
E-mail address: kzfung@mail.ncku.edu.tw (K.-Z. Fung).

0378-7753/$ – see front matter © 2004 Elsevier B.V. All rights reserved.
doi:10.1016/j.jpowsour.2003.12.062

use as the electrolyte materials for intermediate-temperature (<800 °C) SOFCs. Recent work by Ishihara et al. [5] has shown that the substitution of divalent cations, like Ca, Sr, Ba, and/or Al, In, Mg, etc. for La^{3+} and/or Ga^{3+} in the $LaGaO_3$ effectively enhances the oxide ion conductivity. Similar result was also observed by Goodenough and co-workers [8,9], and Kim et al. [10]. Furthermore, the $LaGaO_3$-based perovskite-type oxidefs have ionic transport numbers close to unity, exhibit large electrolytic domains and are insensitive to moisture. These are essential characteristics for an electrolyte material in high temperature fuel cells.

However, the high cost of gallium compounds and their low mechanical strength are the main obstacles for using doped $LaGaO_3$ in SOFC application. Therefore, the replacement of Ga with inexpensive element, such as Al, is highly desirable. It was found that the conductivity of $LaAlO_3$ was significantly affected by the addition of aliovalent cations. Rare-earth aluminates such as $(Ln_{1-x}M_x)AlO_{3-\delta}$ or $Ln(Al_{1-y}M_y)O_{3-\delta}$ (M: Mg^{2+}, Ca^{2+}, Sr^{2+}) show higher conductivity than that of $LnAlO_3$ [12–22]. Among these aluminates, Ca- and Ga-doped $NdAlO_3$ systems were found to exhibit the highest conductivity of about 0.0398 S/cm at 950 °C based on the work of Ishihara [23]. The possibility of using aluminate-based materials as electrolytes for SOFC has also been suggested by Takahashi and Iwahara [21].

Even though both of $LaAlO_3$ and $LaGaO_3$ have similar perovskite-based structure, our preliminary work showed that the solubility of foreign cations varied considerably between these two materials. Thus, the objective of this work was to study the difference in dissolution behavior and conductivity for doped $LaAlO_3$ and $LaGaO_3$ systems when both Sr and Mg were used as the dopants.

In the present study, various amounts of SrO and MgO were added into $LaAlO_3$ and $LaGaO_3$ by repeated calcination and mixing. Undoped and doped $LaAlO_3$ and $LaGaO_3$ were characterized by XRD, which were used for the structural analysis. The ac impedance technique was used to determine the electrical conductivity of sintered samples at various temperatures.

2. Experimental procedure

$LaAlO_3$ and $LaGaO_3$ with and without dopant(s) were synthesized using the solid-state reaction method. Due to the hygroscopic nature of La_2O_3, La_2O_3 was heated to 1000 °C for 1 h prior to the weighing process. TGA was also conducted on all raw materials to confirm the accuracy of the weighing procedure. The stoichiometric ratio of La_2O_3 (Strem, 99.9%), Ga_2O_3 (Alfa, 99.999%), $Mg(NO_3)_2{\cdot}6H_2O$ (Showa, 99.0%), and $Sr(NO_3)_2$ (Showa, 98.0%) were weighed and ball-milled with ethanol (99.8%) for 24 h. The slurry was then dried, reground in an agate mortar and sieved through a 200 mesh sieve. The powder mixture was calcined at 1373 K for 24 h in air. The calcined powder was pulverized again with a pestle and mortar and then reground using ball-milling again. The powder was then pressed into several circular disks of 25 mm diameter and 4 mm thickness using uniaxial die pressing at 30 MPa, followed by cold isostatic pressing under a pressure of 200 MPa. The samples were then sintered at 1773 K for 3 h in air with a heating rate of 2 °C/min. In order to examine the dissolution of various dopants in $LaGaO_3$ and $LaAlO_3$, the crystal structures of the undoped and doped samples were analyzed using Regaku D/MaxIII. VX-R X-ray system. The surface layers of sintered samples were removed before the XRD examination. The Cu Kα radiation was used and the scanning rate was set at 2°/min with a 2θ range between 20 and 80°. For the determination of lattice parameters, a slow scanning rate of 0.25°/min was used. The lattice parameters were refined using the least-square method. To investigate the effect of aliovalent cations on the ionic conductivity, the conductivity of undoped and doped $LaAlO_3$ and $LaGaO_3$ samples was measured using the two-probe ac impedance method. Platinum paste was applied on both surfaces of the sintered disks to be used as the electrodes. The platinum paste was fired at 700 °C for 2 h to remove the organic binders. Silver wires were used as the lead wires connected to both electrodes. The impedance of samples were measured over a frequency range between 20 Hz and 1 MHz using an HP-4284A LCR meter. The electrical conductivity of sintered samples was then measured as a function of temperature from 773 to 1173 K in air. The conductivity was also measured as a function of concentration of various dopants.

3. Results

3.1. Structure analysis of undoped and doped $LaAlO_3$

3.1.1. $LaAlO_3$-based system

XRD traces for undoped and doped $LaAlO_3$ after heated at 1500 °C for 3 h are given in Fig. 1a–e. Fig. 1a shows a single rhombohedral structure obtained from the undoped $LaAlO_3$. Fig. 1b shows the XRD traces of $LaAlO_3$ doped with 10% MgO for the substitution of B-site cations (i.e. Al). For 10% Mg-doped $LaAlO_3$, a second phase was observed. The extra reflections from the second phase are consistent with those of $La_4Al_2MgO_{10}$ (JCPDS: 43-0922). This result indicates that the solubility of MgO in $LaAlO_3$ should be less than 10%. The observation of second phase in Mg-doped $LaAlO_3$ were also shown by Nguyen [15] and Lybye et al. [19]. Although a slightly higher solubility of MgO in $LaAlO_3$ was reported by Nguyen [15], the discrepancy may be caused by the difference in the synthesis route between the low-temperature “Pechini process” and high-temperature “solid-state reaction.” The XRD traces of $LaAlO_3$ doped with 20 and 30% SrO are were shown in Fig. 1c and d. In 30% Sr-doped $LaAlO_3$, the second phase of $LaSrAlO_4$ (JCPDS: 24-1125) was observed. This result

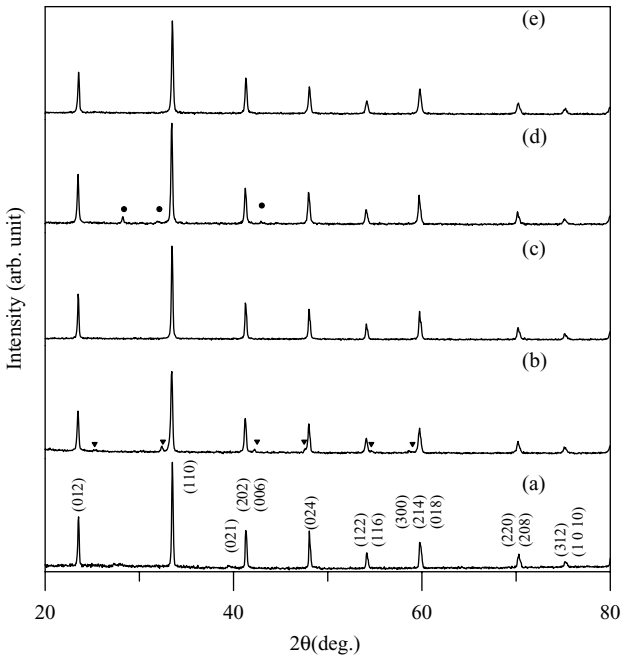

Fig. 1. XRD trace for (a) undoped $LaAlO_3$ and Mg/Sr doped $LaAlO_3$ with the addition of (b) 10% Mg, (c) 20% Sr, (d) 30% Sr, and (e) 10% Sr and 10% Mg synthesized at 1500 °C for 3 h. The second phases observed were $La_4Al_2MgO_{10}$ (marked as (▼)) and $LaSrAlO_4$ (marked as (●)).

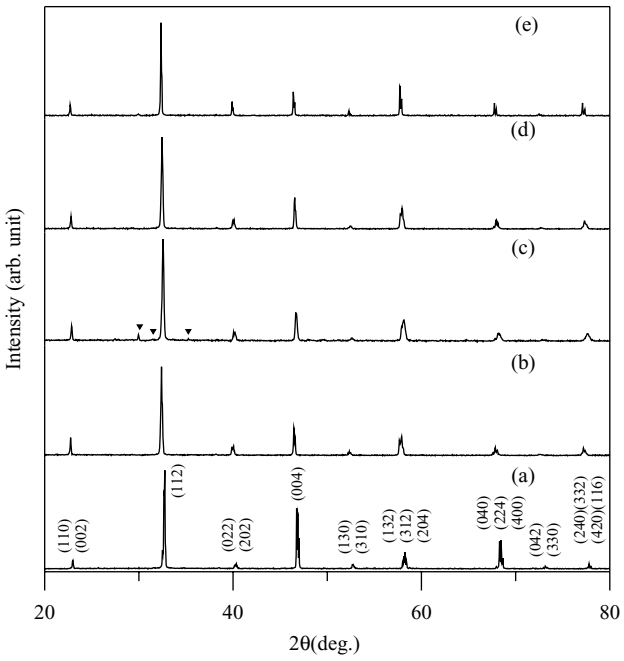

Fig. 2. XRD trace for (a) undoped $LaGaO_3$ and Mg/Sr-doped $LaGaO_3$ with the addition of (b) 10% Mg, (c) 10% Sr, (d) 10% Sr–10% Mg, and (e) 20% Sr–20% Mg synthesized at 1500 °C for 3 h. The second phase observed was $LaSrGa_3O_7$ (marked as (▼).

indicates that the solubility of Sr ions in the A-site cation sublattice of $LaAlO_3$ is between 20 and 30%. Same solubility range was also reported by Nguyen [15] and Lybye et al. [19] et al. In doubly-doped $LaAlO_3$, the dissolution behavior observed is different from the singly-doped samples. In 10% Sr–10% Mg doubly-doped $LaAlO_3$, a single rhombohedral phase was also obtained while the second phase of $La_4Al_2MgO_{10}$ found in the 10% Mg-doped $LaAlO_3$ was not observed. Therefore, in the doubly-doped $LaAlO_3$, the solubility of one dopant was affected by the presence of another dopant as shown in Fig. 1e.

3.1.2. $LaGaO_3$-based system

Unlike the doped-$LaAlO_3$ system, the X-ray analysis of $LaGaO_3$ gives completely different dissolution behavior. As shown in Fig. 2a, undoped $LaGaO_3$ also exhibits single-phase orthorhombic structure after samples were processed under the same conditions as $LaAlO_3$. For Mg-doped $LaGaO_3$ shown in Fig. 2b, no trace of the second phase was found after 20% of MgO was added. Ishihara et al. [5] also showed the same solubility limit of MgO (∼20%) in $LaGaO_3$. For Sr-doped $LaGaO_3$, the solubility of SrO was, however, less than 10 mol% and a small amount of second phase, $LaSrGa_3O_7$ (JCPDS: 45-0637), was detected as shown in Fig. 2c. Same trend was also reported by Huang et al. [6]. From these results, it is clear that SrO is less soluble than MgO in $LaGaO_3$. For the doubly-doped $LaGaO_3$, the solubility of one dopant was also affected by the presence of another dopant. Interestingly, when 10% MgO and 10% SrO were added into $LaGaO_3$ simultaneously, the second phase that originally was found in 10% Sr-doped $LaGaO_3$ disappeared as shown in Fig. 2c. It is evident that the solubility of SrO was enhanced by adding MgO simultaneously into $LaGaO_3$. For 20% Sr–20% Mg doubly-doped $LaGaO_3$, the dissolution of Sr ions was significantly enhanced by the simultaneous addition of 20% MgO and 20% SrO. Consequently, a single phase of perovskite was observed in Fig. 2e.

3.2. Conductivity measurement

3.2.1. $LaAlO_3$-based system

Fig. 3 shows plots of $\ln(\sigma T)$ versus $1000/T$ for $LaAlO_3$-based oxides at temperatures ranging from 500 to 900 °C in air. Among them, the undoped $LaAlO_3$ sample exhibits the lowest conductivity of 2×10^{-4} S/cm at 800 °C. For doped $LaAlO_3$, the conductivities were drastically enhanced by the addition of divalent dopants, SrO and/or MgO. For instance, the sample of 20% Sr-doped $LaAlO_3$ shows improved conductivity of 5×10^{-3} S/cm at 800 °C. For 10% Mg-doped and 10% Sr-10% Mg doubly-doped $LaAlO_3$, the conductivities measured were 1.7×10^{-3} and 4.3×10^{-3} S/cm at 800 °C, respectively. Although all of these values are significantly higher than undoped $LaAlO_3$, they are lower than that of 20% Sr-doped $LaAlO_3$. It was suspected that the presence of second phase had an adverse effect on the conductively of overly-doped $LaAlO_3$. To determine the conductivities of second phases, stoi-

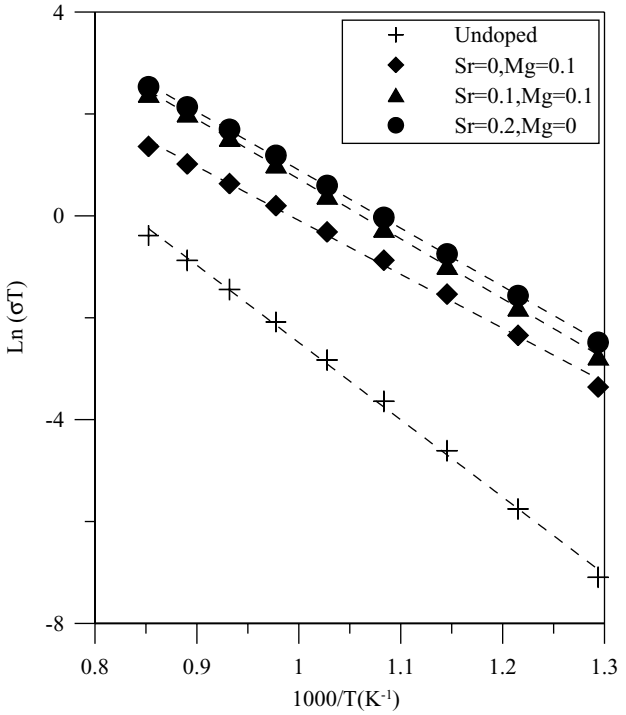

Fig. 3. Conductivity of undoped and doped $LaAlO_3$ plotted as a function of 1000/*T*.

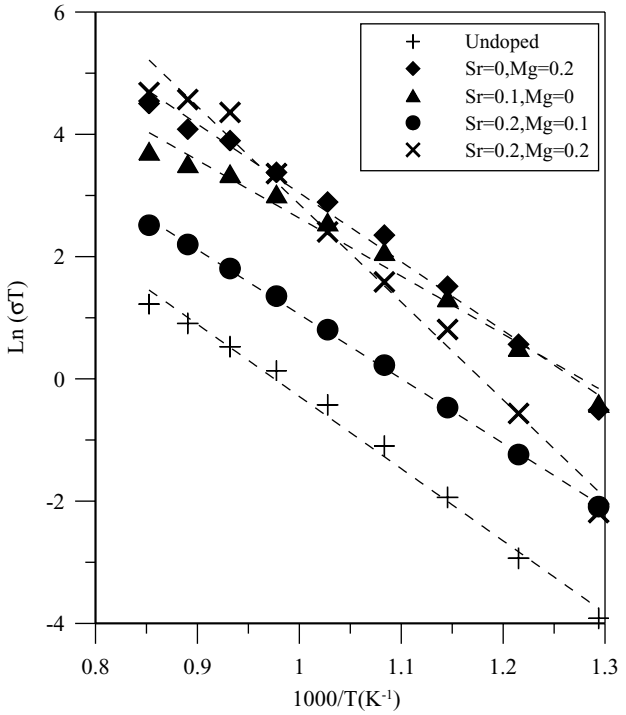

Fig. 4. Conductivity of undoped and doped $LaGaO_3$ plotted as a function of 1000/*T*.

chiometric compounds of $La_4Al_2MgO_{10}$ and $LaSrAlO_4$ were fabricated and then the conductivity measurement was conducted. The conductivities for $La_4Al_2MgO_{10}$ and $LaSrAlO_4$ were found to be as low as 3.4×10^{-4} and 2.7×10^{-4} S/cm, respectively. Thus, the decline in the conductivities of 10% Mg-doped and doubly-doped 10% Mg–10% Sr $LaAlO_3$ was caused by the presence of low-conductivity second phases.

3.2.2. *$LaGaO_3$-based system*

Fig. 4 shows the results of conductivity measurement for undoped, Sr- and/or Mg-doped $LaGaO_3$ systems at temperatures ranging from 500 to 900 °C in air. Similar to the $LaAlO_3$ systems, all doped-$LaGaO_3$ samples exhibit higher conductivity than undoped $LaGaO_3$. The undoped $LaGaO_3$ exhibits the lowest conductivity of 1.6×10^{-3} S/cm at 800 °C. The ionic conductivity of doped-$LaGaO_3$ also increased as the concentration of divalent dopant increased until the second phase appeared. For 10% Sr doped $LaGaO_3$, the conductivity measured was 2.7×10^{-2} S/cm. For 20% Mg doped $LaGaO_3$, the conductivity was enhanced to 4.6×10^{-2} S/cm. For 20% Sr–20% Mg doubly-doped $LaGaO_3$, the conductivity reached 7.3×10^{-2} S/cm at 800 °C which is four times as high as that of YSZ. When the second phase appeared in the heavily doped $LaGaO_3$, for instance, 20% Sr–10% Mg doubly-doped $LaGaO_3$, a decrease in conductivity was also observed. The conductivities for the second phases, $LaSrGaO_4$ and $LaSrGa_3O_7$ were found to be 8.2×10^{-4} and 8.8×10^{-4} S/cm which were also considerably lower than undoped $LaGaO_3$.

4. Discussion

4.1. *Structure variation between of $LaAlO_3$ and $LaGaO_3$*

In $LaAlO_3$ and $LaGaO_3$ perovskites, La ions tend to occupy A-site positions and Al and Ga cations occupy B-site positions due to the difference in their ionic radii. The ionic radii for cations and oxygen ions used in this study are adopted from Shannon's work [24]. Based on the ionic radii of cations and oxygen ions ($r_{Al^{3+}} = 0.535$ Å, $r_{Ga^{3+}} = 0.62$ Å, $r_{La^{3+}} = 1.36$ Å, and $r_{O^{2-}} = 1.40$ Å) [24], the tolerance factor for a $LaAlO_3$ lattice was calculated to be 1.009. On the other hand, for $LaGaO_3$, the tolerance factor was found to be 0.966. For a cubic perovskite, the tolerance factor usually falls in the range between 0.95 and 1.0. Therefore, $LaAlO_3$ forms a rhombohedral structure consisting of four slightly distorted pseudo-cubic perovskite subcells. $LaGaO_3$, on the other hand, crystallized in a less-symmetric orthorhombic structure which also consists of perovskite subcells [25]. The resemblance between the rhombohedral $LaAlO_3$ and pseudo-cubic perovskite can be further illustrated from the theoretical intensity calculation as shown in Tables 1 and 2. These results show an excellent agreement with the observed intensities from Figs. 1 and 2. The difference in the relative intensities between $LaAlO_3$ and $LaGaO_3$

is due to the variation in atomic scattering factor from Al and Ga ions. Although $LaAlO_3$ and $LaGaO_3$ have similar perovskite structure, the solubility of aliovalent dopants, SrO and MgO, show completely different results. These results can be rationalized based on the difference in bonding characteristics and ionic radius between doping ions and parent cations.

4.2. Effect of ionic radius

For the addition of SrO and MgO in both $LaAlO_3$ and $LaGaO_3$ systems, Mg is less soluble in $LaAlO_3$ than in $LaGaO_3$. On the contrary, Sr ion is more tolerant in $LaAlO_3$ than in $LaGaO_3$. The ionic radius of Mg ion is 34.6% ($r_{Mg^{2+}} = 0.72$ Å) larger than that of Al ion. The lattice parameter of pseudo-cubic $LaAlO_3$ (~3.79 Å) is also smaller than pseudo-cubic $LaGaO_3$ (~3.89 Å). Hence, Mg ions would not be easily tolerated in $LaAlO_3$ structure and may segregate or form a second phase, $La_4Al_2MgO_{10}$. Compared with the ionic radius of Ga ions, Mg ion is only 16% larger. Thus, higher solubility of MgO in $LaGaO_3$ (~20 mol%) than that in $LaAlO_3$ (<10 mol%) is expected. It is interesting to note that the dissolution of Sr ion in the larger $LaGaO_3$ lattice is more difficult than that in the smaller $LaAlO_3$ lattice. The difference in SrO solubility between $LaGaO_3$ and $LaAlO_3$ may be caused by the extent of structure distortion. From the calculation of tolerance factor, t, it may be concluded that $LaAlO_3$ ($t = 1.009$) is closer to the ideal (cubic) perovskite than $LaGaO_3$ ($t = 0.966$). In $LaGaO_3$, the interatomic distance between O and La varied from 2.46 to 3.14 Å [26]. Particularly, the O–La distance along [1, −1, 1] and [−1, 1, −1] is less than the sum of $r_{La^{3+}}$ and $r_{O^{2-}}$ as shown in Fig. 5. This result suggests that it will be less favorable for larger

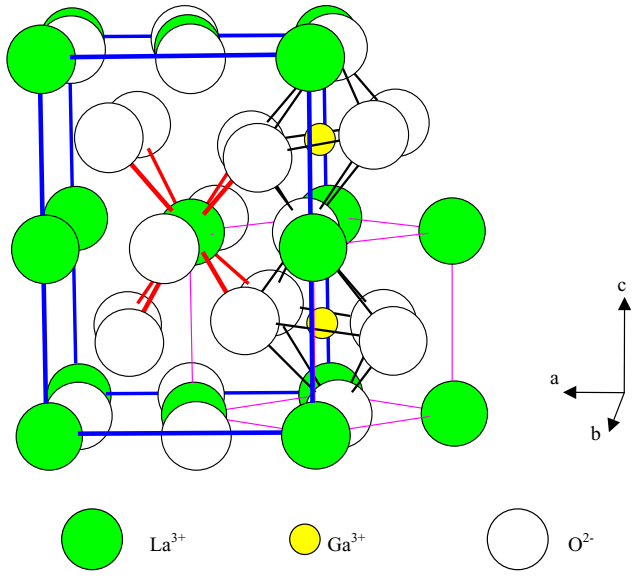

Fig. 5. Schematic diagram of orthorhombic $LaGaO_3$ with tilting GaO_6 octahedra.

Table 1
The calculated relative intensities for diffracted reflection from $LaAlO_3$

h	k	l	2θ	f_{La}	f_{Al}	f_O	F^2	Lorentz-polarization factor	Multiplicity factor	Intensity	Relative I (%)
Based on orthorhombic lattice			Based on pseudo-cubic lattice								
0	1	2	1 0 0	23.46	50.36	9.44	7.20	1137.038	45.516	6	310521.008	48.85
1	1	0	1 1 0	33.42	45.54	9.01	5.84	2471.084	21.436	12	635636.318	100.00
2	0	2	1 1 1	41.23	43.80	8.59	5.02	1618.453	13.494	8	174720.077	27.49
0	0	6										
0	2	4	2 0 0	47.98	41.57	8.20	4.41	2935.472	9.590	6	168911.406	26.57
1	2	2	2 1 0	54.07	39.62	7.86	3.89	776.737	7.306	24	136188.960	21.43
1	1	6										
3	0	0	2 1 1	59.73	38.02	7.53	3.54	1764.840	5.834	24	247101.786	38.87
2	1	4										
0	1	8										
2	2	0	2 2 0	70.19	35.27	6.96	2.99	2044.848	4.122	12	101153.311	15.91
2	0	8										
3	1	2	3 0 0	75.15	34.03	6.70	2.75	604.176	3.616	6	13107.968	2.06
1	0	10	2 2 1	75.15	34.03	6.70	2.75	604.176	3.616	24	52431.870	8.25
1	2	8	3 1 0	80.00	33.11	6.45	2.60	1366.042	3.255	24	106703.876	16.79

Table 2
The calculated relative intensities for diffracted reflection from $LaGaO_3$

$h\,k\,l$													
Based on orthorhombic lattice			Based on pseudo-cubic lattice			2θ	f_{La}	f_{Ga}	f_O	F^2	Lorentz-polarization factor	Multiplicity factor	Intensity	Relative I (%)
1	1	0	1	0	0	22.81	50.61	26.52	7.29	282.240	48.245	6	81700.530	7.06
0	0	2												
1	1	2	1	1	0	32.48	46.90	24.13	5.96	4234.105	22.788	12	1157849.284	100.00
0	2	2	1	1	1	40.06	44.20	22.41	5.12	724.148	14.381	8	83312.377	7.20
2	0	2												
0	0	4	2	0	0	46.60	42.03	21.03	4.54	4569.760	10.242	6	280821.986	24.25
1	3	0	2	1	0	52.49	40.12	19.82	4.02	265.038	7.812	24	49693.790	4.29
3	1	0												
1	3	2	2	1	1	57.95	38.51	18.90	3.64	2891.213	6.240	24	433012.761	37.40
3	1	2												
2	0	4												
2	2	4	2	2	0	68.02	35.83	17.53	3.11	3188.861	4.395	12	168166.616	14.52
4	0	0												
0	4	2	3	0	0	72.77	34.62	16.92	2.86	220.226	3.838	6	5071.670	0.44
3	3	0	2	2	1	72.77	34.62	16.92	2.86	220.226	3.838	24	20286.678	1.75
2	4	0	3	1	0	77.41	33.56	16.38	2.66	2235.398	3.433	24	184175.581	15.91
3	3	2												
4	2	0												
1	1	6												

doping ions, like Sr to dissolve in the A-site of $LaGaO_3$ perovskite lattice. On the other hand, the interatomic distance between Al and La in a $LaAlO_3$ lattice is close to 2.68 Å [27] which is more suitable for the occupancy of Sr. Therefore, the SrO tends to be less soluble in $LaGaO_3$ than in $LaAlO_3$.

The additional cause for the difference in Sr solubility between $LaGaO_3$ and $LaAlO_3$ may be the electrostatic repulsion between cations. Since $LaAlO_3$ and $LaGaO_3$ can be viewed as pseudo-cubic perovskites, the corresponding lattice constants are 3.791 and 3.897 Å. However, the difference between lattice constants of $LaAlO_3$ and $LaGaO_3$ (0.106 Å) is less than that between sizes of Ga and Al ions (0.17 Å). These results indicate that the interatomic distance between La ion and Ga ion in $LaGaO_3$ is closer than that between La ion and Al ion. Since Sr ion has larger ionic radius than La ions, it is reasonable to expect that the repulsion between Sr/La and Ga ions be stronger than that between Sr/La and Al ions. Thus, Sr ions will be less tolerant in the A-site position of $LaGaO_3$ perovskite.

4.3. Effect of doubly-doping on dissolution behavior of $LaAlO_3$ and $LaGaO_3$

In the doubly-doped $LaGaO_3$ samples, the addition of MgO enhances the solubility of SrO. However, in doubly-doped $LaAlO_3$, the addition of Mg suppresses the dissolution of Sr. These results may be explained by the bonding characteristics of the ABO_3 lattice. It is known that the oxides with stronger bond strength exhibit higher melting points. The melting point of $LaAlO_3$ was reported to be 2110 °C [13] while the melting point of $LaGaO_3$ was only 1720 °C [28]. Since both $LaAlO_3$ and $LaGaO_3$ have similar structure and atomic coordination, the higher melting point of $LaAlO_3$ than $LaGaO_3$ is caused by stronger bond strength between Al and O than Ga and O. It was also found that the bond distance between Al and O, 1.895 Å [27], is less than that between Ga and O (1.98 Å) [29]. Thus, the $LaGaO_3$ lattice may be easily expanded by the addition of Mg ions. Consequently, the solubility of SrO in 20% Mg-doped $LaGaO_3$ was enhanced from 10 to 20%. On the other hand, the $LaAlO_3$ lattice could not be easily expanded by the addition of MgO, because of the stronger bonding strength between Al and O. Thus, the solubility of Sr in Mg-doped $LaAlO_3$ was suppressed from 20 to 10%.

4.4. Effect of $LaAlO_3$ and $LaGaO_3$ lattices on conductivity

In Figs. 3 and 4, the conductivity was plotted as a function of the inverse of temperature for undoped and doped $LaAlO_3$ and $LaGaO_3$. The conductivity of $LaAlO_3$ is much lower than that of $LaGaO_3$ at the same temperature range. Since the bonding strength of Al–O is much higher than Ga–O, the formation of intrinsic oxygen vacancies through the thermally-activated process would be more difficult in $LaAlO_3$ than in $LaGaO_3$. The smaller lattice of undoped

$LaAlO_3$ also has an adverse effect on the migration of oxygen ions. Thus, the undoped $LaAlO_3$ exhibits a conductivity of one order of magnitude lower than the undoped $LaGaO_3$.

4.5. Effect of divalent dopants on ionic conduction

In the doped $LaAlO_3$ and $LaGaO_3$ systems, the conductivity measurement clearly showed that the conductivity was enhanced by the addition of SrO and MgO on both $LaGaO_3$ and $LaAlO_3$ when the concentration of dopants was within the solubility limit. The addition of SrO and MgO may be incorporated into the $LaAlO_3$/$LaGaO_3$ lattice according to the following defect reactions:

$$2SrO + Al_2O_3/Ga_2O_3 \xrightarrow[LaAlO_3/LaGaO_3]{} 2Sr'_{La} + 2Al^x/Ga^x_{Al/Ga} + 5O_O{}^x + V_O{}^{\bullet\bullet} \quad (1)$$

$$2MgO + La_2O_3 \xrightarrow[LaAlO_3/LaGaO_3]{} 2Mg'_{Al/Ga} + 2La_{La}{}^x + 5O_O{}^x + V_O{}^{\bullet\bullet} \quad (2)$$

where the defect notation of Kröger and Vink was adopted.

When the Sr ion substitutes for the A-site cation sublattice in $LaAlO_3$ or $LaGaO_3$, the negative charge of Sr'_{La} is compensated by the formation of positively charged oxygen vacancy, $V_O{}^{\bullet\bullet}$.

In other words, the oxygen vacancies are created by the substitution of Sr for La. Thus, the concentration of oxygen vacancy increases as the concentration of SrO dopant increases. Similarly, the substitution of Mg for Al or Ga is also compensated by the formation of oxygen vacancy. Therefore, the enhancement in ionic conductivity is expected when the divalent dopant MgO or SrO is dissolved into the $LaAlO_3$ or $LaGaO_3$ lattice. For doubly-doped $LaAlO_3$ and $LaGaO_3$ samples, the oxygen vacancies can be further generated by the addition of divalent dopants on both A-site and B-site cation sublattices. Therefore, the higher conductivity was observed in 10% Sr–10% Mg doubly-doped $LaAlO_3$ and 20% Sr–20% Mg doubly-doped $LaGaO_3$.

After the dopant concentration exceeded the solubility limit, the second phase appeared. In excessively doped $LaAlO_3$ sample, the second phases were found to be $La_4Al_2MgO_{10}$ and $LaSrAlO_4$. In excessively doped $LaGaO_3$ samples, the second phases observed are $LaSrGa_3O_7$ and $LaSrGaO_4$. Among these second phases, $LaSrAlO_4$ and $LaSrGaO_4$ have the same tetragonal structure. $La_4Al_2MgO_{10}$ and $LaSrGa_3O_7$ exhibit complex orthorhombic and tetragonal structures, respectively. These structures are different from the perovskites structure and exhibit low conductivities. Furthermore, the stoichiometric ratio in the perovskite phase was significantly affected by the presence of second phases because the second phases contain La, Al, and Ga cations. For example, in 30% Sr doped $LaAlO_3$, the excess Sr resulted in the formation of $LaSrAlO_4$. Then, La and Al must be depleted from the Sr-containing $LaAlO_3$. Then, the cation vacancies may be formed and the conduction of oxygen ions may be suppressed. Therefore, the conductivity of excessively doped $LaAlO_3$ was drastically suppressed by the segregation of $LaSrAlO_4$. Similar behavior was also observed in the $LaGaO_3$ system. When the second phase appeared, the conductivity of heavily doped $LaGaO_3$ was also significantly reduced. Finally, a maximum in conductivity was obtained when the dopant concentration reaches the solubility limit.

4.6. Effect of divalent dopants on activation energy

Table 3 lists the activation energies for ionic conduction in undoped and doped $LaAlO_3$ and $LaGaO_3$.

4.6.1. Undoped $LaGaO_3$ and $LaAlO_3$

The activation energy for undoped $LaAlO_3$ is as high as 125.28 kJ/mol. For undoped $LaGaO_3$, the activation energy was estimated to be 98.47 kJ/mol. In undoped $LaAlO_3$ and $LaGaO_3$, the oxygen ion conduction can be achieved by movement of oxygen ions through intrinsically induced oxygen vacancies. Thus, the activation energies for undoped samples must include the enthalpy for formation of oxygen vacancies as well as the enthalpy for the migration of oxygen ions. Thus, the undoped $LaAlO_3$ and $LaGaO_3$ exhibit higher activation energies than doped ones. Furthermore, the higher activation energy of undoped $LaAlO_3$ than $LaGaO_3$ is caused by stronger bonding and smaller lattice.

Table 3
The r_{crit} (Å) and activation energy (kJ/mol) of undoped/doped $LaAlO_3$ and $LaGaO_3$ systems

System	r_{crit} (Å)	E_a (kJ/mol)
$LaAlO_3$		
$LaAlO_3$	0.9058	125.28
$La_{0.9}Sr_{0.1}AlO_{3-\delta}$	0.9016	78.80
$La_{0.8}Sr_{0.2}AlO_{3-\delta}$	0.8972	94.86
$LaAl_{0.9}Mg_{0.1}O_{3-\delta}$	0.8996	87.91
$La_{0.9}Sr_{0.1}Al_{0.9}Mg_{0.1}O_{3-\delta}$	0.8969	97.50
$La_{0.8}Sr_{0.2}Al_{0.9}Mg_{0.1}O_{3-\delta}$	0.8933	104.62
La $Al_{0.8}Mg_{0.2}O_{3-\delta}$	0.8966	93.54
$La_{0.9}Sr_{0.1}Al_{0.8}Mg_{0.2}O_{3-\delta}$	0.8911	96.12
$La_{0.8}Sr_{0.2}Al_{0.8}Mg_{0.2}O_{3-\delta}$	0.8878	110.10
$LaGaO_3$		
$LaGaO_3$	0.9326	98.47
$La_{0.9}Sr_{0.1}GaO_{3-\delta}$	0.9373	92.78
$La_{0.8}Sr_{0.2}GaO_{3-\delta}$	0.9388	69.09
$LaGa_{0.9}Mg_{0.1}O_{3-\delta}$	0.9292	83.28
$La_{0.9}Sr_{0.1}Ga_{0.9}Mg_{0.1}O_{3-\delta}$	0.9282	80.40
$La_{0.8}Sr_{0.2}Ga_{0.9}Mg_{0.1}O_{3-\delta}$	0.9296	77.98
$LaGa_{0.8}Mg_{0.2}O_{3-\delta}$	0.9176	92.76
$La_{0.9}Sr_{0.1}Ga_{0.8}Mg_{0.2}O_{3-\delta}$	0.9195	96.86
$La_{0.8}Sr_{0.2}Ga_{0.8}Mg_{0.2}O_{3-\delta}$	0.9216	132.90

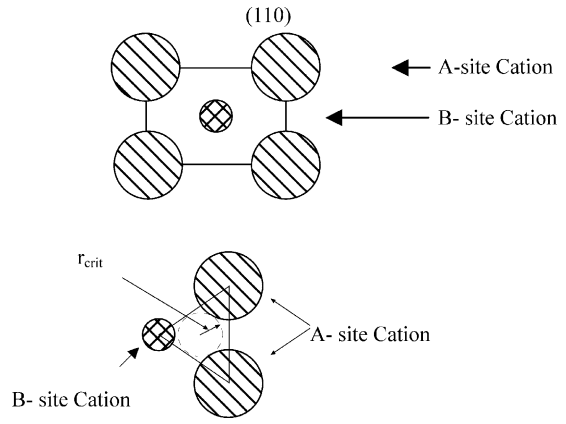

Fig. 6. Schematic diagrams showing how the critical radius is determined from the space available for oxygen ion migration through the (1 1 0) plane.

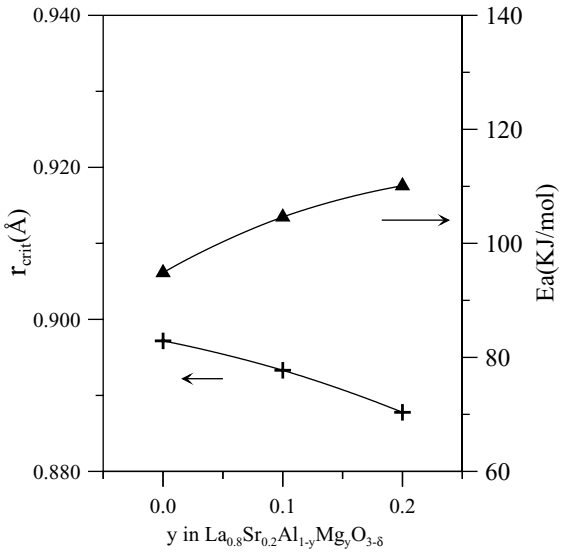

Fig. 7. The activation energy and critical radius plotted as a function of Mg site-fraction in $La_{0.8}Sr_{0.2}Al_{1-y}Mg_yO_{3-\delta}$.

4.6.2. Singly doped $LaAlO_3$ and $LaGaO_3$

The activation energies for ionic conduction in $LaAlO_3$ and $LaGaO_3$ systems were also influenced by the addition of dopants. For doped $LaAlO_3$ and $LaGaO_3$, the variation of activation energy as a function of dopant concentration can be illustrated using the critical radii for the migration of oxygen ions [20].

With the addition of SrO or MgO into $LaAlO_3$, the activation energies were reduced to 78.80–87.91 kJ/mol. The reduced activation energy of doped $LaAlO_3$ can be attributed to the formation of oxygen vacancies for the charge compensation of lower-valent dopants. Thus, the concentration of oxygen vacancies was extrinsically fixed by the addition of lower valent cation ions according to Eqs. (1) and (2). In additions, the activation energy of Mg-doped $LaAlO_3$ is lower than Sr-doped $LaAlO_3$. Same results were also observed by Kliner et al. [22]. It was proposed that the association energy between oxygen vacancy and the dopant $(M'_{Al} - V_O^{\bullet\bullet} - M'_{Al})$, is higher in Sr-doped $LaAlO_3$ than in Mg-doped $LaAlO_3$. Comparison the activation energy of $LaAlO_3$ and $LaGaO_3$, $LaAlO_3$ systems exhibits slightly higher activation energy.

4.6.3. Doubly-doped $LaAlO_3$ and $LaGaO_3$

Since both $LaGaO_3$ and $LaAlO_3$ exhibit pseudo-cubic perovskite structure, for simplicity, both of them are treated a the cubic perovskite. The schematic diagram of (1 1 0) plane is shown in Fig. 6 where the large circles represent the A-site cations and the small circles represent the B-site cations. The possible path for oxygen transport along ⟨1 1 0⟩ edge of the BO_6 (B: Ga, Al) octahedron would be the free space surrounded by two A-site cations and one B-site cation. A critical radius, r_{crit}, can be determined based on the space available for each system. The critical radius can be expressed as follows [20]:

$$r_{crit} = \frac{a_0((3/4)a_0 - \sqrt{2}r_B) - [(r_A - r_B)(r_A + r_B)]}{[2(r_A - r_B) + \sqrt{2}a_0]} \quad (3)$$

For doubly-doped $LaAlO_3$ and $LaGaO_3$, the variation of activation energies as a function of dopant concentration can be illustrated using the calculated critical radii for the migration of oxygen ions. When the r_{crit} increases, the activation energy for oxygen transport is expected to be smaller. On the other hand, the r_{crit} decreases, the activation energy for oxygen transport is expected to be larger.

Fig. 7 shows that the variation of r_{crit} and activation energy on 20% Sr-doped $LaAlO_3$ was plotted as a function of MgO concentration. As the concentration of MgO increases, the value of r_{crit} decreases and oxygen transport becomes more difficult. Thus, the activation energy for ionic conduction increases with the increasing concentration of MgO. Fig. 8 shows that r_{crit} still decreases as the SrO concentration increases when MgO concentration remains at 10%. Thus, the activation energy for ion transport is also increased.

In the case of $LaGaO_3$, when the concentration of SrO is fixed at 20%, the calculated r_{crit} in the $LaGaO_3$ lattice decreases as the concentration of MgO co-dopant increases. Thus, the activation energy for ionic conduction increases from 69.09 to 132.90 kJ/mol when the concentration of MgO increase from 0 to 20%. On the contrary, when the concentration of MgO dopant (for B-cation sublattice) is fixed at 10%, the calculated r_{crit} in the $LaGaO_3$ lattice increase as the concentration of SrO increases. As a result, the activation energies of oxygen conduction slightly changed from 83.28 kJ/mol, 80.40 kJ/mol to 77.98 kJ/mol, for the samples of singly-doped $LaGa_{0.9}Mg_{0.1}O_{3-\delta}$, doubly-doped $La_{0.9}Sr_{0.1}Ga_{0.9}Mg_{0.1}O_{3-\delta}$ and $La_{0.8}Sr_{0.2}Ga_{0.9}Mg_{0.1}O_{3-\delta}$, respectively. From Figs. 7–10, it is evident that the activation energy of ionic conduction is strongly affected by r_{crit}.

The variation of r_{crit} can be rationalized on the change of the corresponding lattice. The increase of r_{crit} with the SrO

addition in $LaGaO_3$ can be explained by the expanded lattice after the addition of Sr ions. As discussed earlier, $LaAlO_3$ has a more rigid lattice. Either Sr or Mg addition has little effect on the expansion of lattice. Thus, the spaces available for oxygen migration become smaller when the larger doping ions are added into the lattice. Hence, it is difficult for oxygen ions to move to adjacent oxygen vacancies and higher activation energy was observed.

5. Conclusions

The following conclusions may be drawn based on the present work:

1. In $LaAlO_3$, less than 10% of MgO was dissolved in the Al-cation sublattice due to the mismatch of ionic radius between Mg and Al ions. On the contrary, as much as 20% of La sites can be replaced by Sr ions. In doubly-doped (Mg^{2+} and Sr^{2+}) $LaAlO_3$, the solubility of SrO was suppressed by the doping of MgO. Only 10% of SrO can be added into 10% Mg-doped $LaAlO_3$. The suppression of SrO solubility may be attributed to the rigidity of $LaAlO_3$ lattice and the electrostatic repulsion between Sr and Mg ions.
2. In doped $LaGaO_3$, the solubility of Mg ion reached 20% without the formation of second phase. For Sr-doped $LaGaO_3$, only 10% of Sr ions were allowed in the $LaGaO_3$ lattice. When 20% of SrO was added into $LaGaO_3$, the second phase of $LaSrGa_3O_7$ was found. In doubly-doped (Mg^{2+} and Sr^{2+}) $LaGaO_3$, the dissolved Mg ions enhanced the solubility of SrO from 10 to 20% due to the expanded lattice.
3. From the conductivities measurement, the oxygen vacancy concentration and ionic conductivity were significantly enhanced when SrO and/or MgO dopants were dissolved into the $LaAlO_3$ and $LaGaO_3$ lattices. However, the conductivity was suppressed when the second phases $LaSrAlO_4$ and $La_4Al_2MgO_{10}$ or $LaSrGaO_4$ and $LaSrGa_3O_7$ were present.
4. The undoped $LaAlO_3$ and $LaGaO_3$ have the highest activation energies than doped ones, respectively. The highest activation energies are contribution from to the enthalpy for formation of oxygen vacancies and the enthalpy for the migration of oxygen ions.
5. In the doped $LaAlO_3$ and $LaGaO_3$ systems, the oxygen migration was affected by the free space available in the lattices or the size of critical radius. In general, the activation energies increased with the increasing concentra-

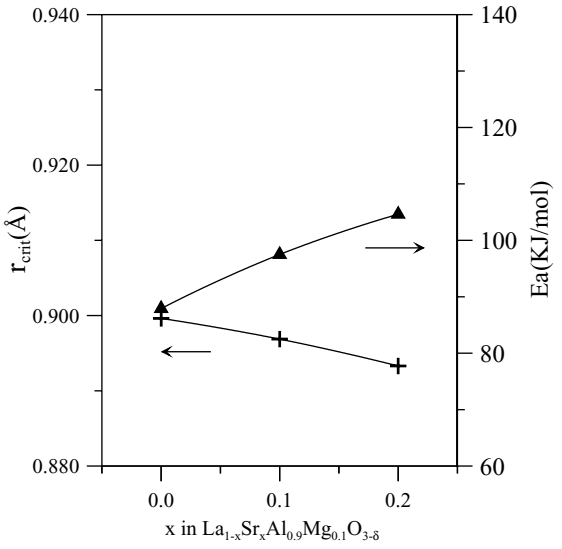

Fig. 8. The activation energy and critical radius plotted as a function of Sr site-fraction in $La_{1-x}Sr_xAl_{0.9}Mg_{0.1}O_{3-\delta}$.

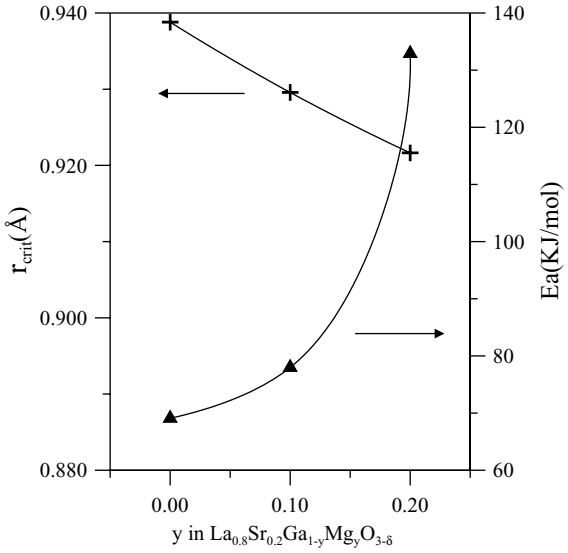

Fig. 9. The activation energy and critical radius plotted as a function of Mg site-fraction in $La_{0.8}Sr_{0.2}Ga_{1-y}Mg_yO_{3-\delta}$.

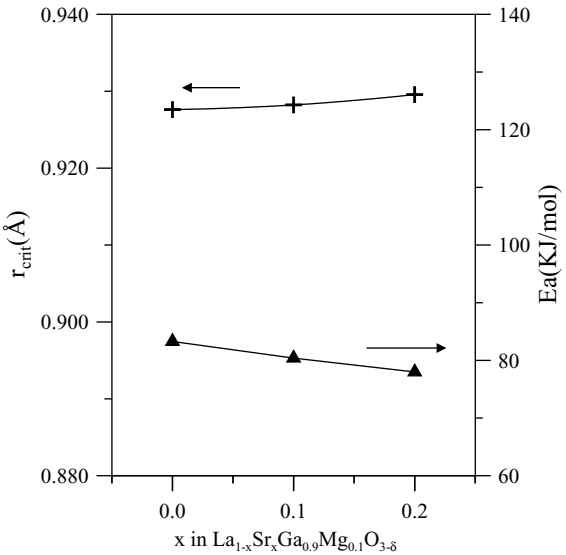

Fig. 10. The activation energy and critical radius plotted as a function of Sr site-fraction in $La_{1-x}Sr_xGa_{0.9}Mg_{0.1}O_{3-\delta}$.

tion of dopants due to the larger ionic radius of doping cations. In Mg-doped $LaGaO_3$, the co-doping of SrO did not change the activation energy noticeably due to nearly unchanged critical radius.

Acknowledgements

This work is financially supported by the National Science Council, Taiwan, Republic of China, under the Grant No. NSC 92-2120-M-006-003.

References

[1] Q. Nguyen, Minh, J. Am. Ceram. Soc. 76 (3) (1993) 563–588.
[2] P. S Badwal, K. Foger, Ceram. Int. 22 (1996) 257–265.
[3] J.N. Pratt, Metall. Transact. 21A (1990) 1223–1245.
[4] H. Inaba, H. Tagawa, Solid State Ionics 83 (1996) 1–295.
[5] T. Ishihara, H. Matsuda, Y. Takita, J. Am. Chem. Soc. 116 (1994) 3801–3803.
[6] P. Huang, A. Petric, J. Electrochem. Soc. 143 (5) (1996) 1644–1648.
[7] J.W. Stevenson, T.R. Armstrong, D.E. McCready, L.R. Pederson, W.J. Weber, J. Electrochem. Soc. 144 (10) (1997) 3613–3620.
[8] K. Huang, R.S. Tichy, J.B. Goodenough, J. Am. Chem. Soc. 81 (1998) 2565–2575.
[9] M. Feng, J.B. Goodenough, K. Huang, C. Milliken, J. Power Sources 63 (1996) 47–51.
[10] S. Kim, M.C. Chun, K.T. Lee, H.L. Lee, J. Power Sources 93 (2001) 279–284.
[11] N. Maffei, A.K. Kuriakose, J. Power Sources 75 (1998) 162–166.
[12] D. Kuscer, M. Hrovat, J. Holc, S. Bernik, D. Kolar, J. Power Sources 71 (1998) 195–198.
[13] C.B. Alcock, J.W. Fergus, L. Wang, Solid State Ionics 51 (1992) 291–295.
[14] J. Mizusaki, I. Yasuda, J.-I. Shimoyama, S. Yamauchi, K. Fueki, J. Electrochem. Soc. 140 (2) (1993) 467–471.
[15] T.L. Nguyen, M. Donkiya, S. Wang, H. Tagawa, T. Hashimoto, Solid State Ionics 130 (2000) 229–241.
[16] P.S. Anderson, G.C. Mather, F.M.B. Marques, D.C. Sinclair, A.R. West, J. Eur. Ceram. Soc. 19 (1999) 1665–1673.
[17] K.W. Browall, O. Muller, Mat. Res. Bull. 11 (1976) 1475–1482.
[18] P.S. Anderson, F.M.B. Marques, D.C. Sinclair, A.R. West, Solid State Ionics 118 (1999) 229–239.
[19] D. Lybye, F.W. Poulsen, M. Morgensen, Solid State Ionic 128 (2000) 91–103.
[20] J.A. Kilner, R.J. Brook, Solid State Ionics 6 (1982) 237–252.
[21] T. Takahashi, H. Iwahara, Energy Convers. 11 (1971) 105.
[22] J.A. Kilner, P. Barrow, R.J. Brook, M.J. Norgett, J. Power Sources 3 (1978) 67–80.
[23] T. Ishihara, H. Matsuda, T. Takita, J. Electrochem. Soc. 141 (12) (1994) 3444–3449.
[24] R.D. Shannon, Acta Cryst. A32 (1976) 751–767.
[25] A.J. Jacobson, B.C. Tofield, B.E.F. Fender, Acta Cryst. B28 (1972) 956.
[26] L. Vasylechko, A. Matkovski, A. Suchocki, D. Savytskii, I. Syvorotka, J. Alloys Compd. 286 (1999) 213–218.
[27] S. Geller, V.B. Bala, Acta Cryst. 9 (1956) 1019–1025.
[28] H.M. O'Bryan, P.K. Gallagher, G.W. Berkstresser, C.D. Brandle, J. Mater. Res. 5 (1) (1990) 183–189.
[29] P.R. Slater, J.T.S. Irvine, T. Ishihara, Y. Takita, J. Solid State Chem. 139 (1998) 135–143.